Magnetic ions exchange interactions in NiO–MgO solid solutions

© N. Mironova-Ulmane, V. Skvortsova, A. Kuzmin, U. Ulmanis, I. Sildos*, E. Cazzanelli**, G. Mariotto***

Institute of Solid State Physics, University of Latvia,
LV-1063 Riga, Latvia
* Institute of Physics, University of Tartu,
EE-2400 Tartu, Estonia
** INFM and Dipartimento di Fisica, Universitá della Calabria,
I-87036 Arcavacata di Rende (Cosenza), Italy
*** INFM and Dipartimento di Fisica, Universitá di Trento,
I-38050 Povo (TN), Italy
E-mail: ulman@latnet.lv

In this work, a review of recent experimental data and their interpretation for $Ni_cMg_{1-c}O$ solid solutions is given. In particular, the influence of exchange interactions between Ni^{2+} ions on the structural, optical, magnetic and vibrational properties is discussed.

This work was partially supported by grants of the Latvian Government (N 01.0806 and 01.0821) and the Estonian Science Foundation (N 3453).

1. Introduction

Solid solutions, in which magnetic ions occupy sites in a face-centred-cubic (fcc) lattice, are of continuous interest during the last decades [1]. Magnetic ordering in these compounds depends on the concentration and site distribution of magnetic ions as well as on the signs and strengths of the nearest-neighbour (NN) J_{NN} and next-nearest-neighbour (NNN) J_{NNN} superexchange interactions [2]. Since superexchange interactions depend on the values of the cation–anion distance and of the cation–anion–cation angle [2], a precise knowledge of the relationship between crystallographic and magnetic structure is important for deep understanding of exchange phenomenon in these materials. In this paper we will review the available experimental data and their interpretation for the case of exchange interactions between Ni^{2+} ions in $Ni_cMg_{1-c}O$ solid solutions.

Pure nickel oxide (NiO) is a classical example of a type-II antiferromagnet having high Nèel temperature $T_N = 523\,\mathrm{K}$ [3]. Below T_N, the spins of the Ni^{2+} ions are ordered ferromagnetically in $\{111\}$ planes, where they lie along the $\langle 112\rangle$ axes [4,5]. Pure NiO has in the paramagnetic phase a rock-salt-type crystal structure with nickel ions located at the center of the NiO_6 octahedra. In the antiferromagnetic (AF) phase, the structure of NiO undergoes a week cubic-to-rhombohedral distortion due to the magnetostriction effect. The AF structure of NiO is determined by dominating superexchange interactions in linear Ni^{2+}–O^{2-}–Ni^{2+} atom chains ($J_{NNN} \approx 150\,\mathrm{cm}^{-1}$) and weak 90° superexchange Ni^{2+}–O^{2-}–Ni^{2+} interactions ($J_{NN} \approx 11\,\mathrm{cm}^{-1}$) [4,6,7]. Second harmonic generation was recently observed in NiO below the Nèel temperature. It is due to the combined magnetic-dipole and electric-dipole transitions between the $3d^8$ levels of the Ni^{2+} ion subject to the crystal field [8].

Substitution of nickel ions by magnesium ions leads to the formation of a continuous series of $Ni_cMg_{1-c}O$ solid solutions and stabilizes the cubic structure [9,10]. A magnetic phase diagram of $Ni_cMg_{1-c}O$ system has been established by elastic magnetic neutron scattering [11] and SQUID magnetometry [11,12]. There are four domains (Fig. 1): (1) a homogeneous antiferromagnet ($0.63 \le c \le 1$); (2) a tricritical region or a frustrated antiferromagnet ($0.04 \le c \le 0.63$); (3) a spin-glass state ($0.25 \le c < 0.4$) and (4) a diamagnet ($c \le 0.2$) [11]. Complementary information on the magnetic ordering in $Ni_cMg_{1-c}O$ single crystals has been obtained from microscopic investigations of the composition and temperature dependence of the domain structure [13]. It was found that the regular domain structure is more sensitive to the concentration of magnesium ions than T_N and appears upon cooling at temperatures well below T_N (dashed line in Fig. 1) [13]. The aforementioned techniques provide rather a macroscopic view on the magnetic structure of solid solutions. In what follows we discuss the experimental results

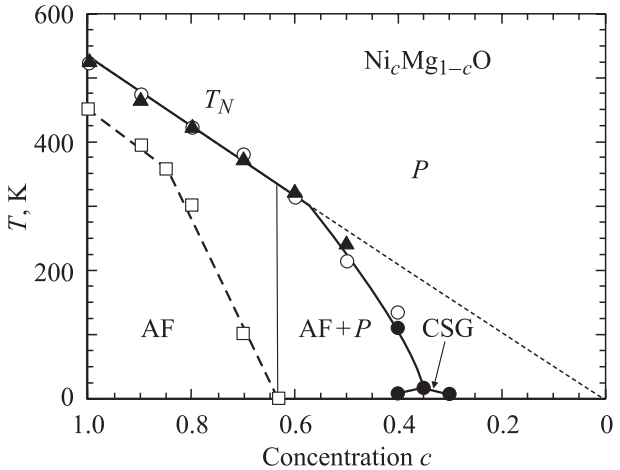

Figure 1. Magnetic phase diagram of $Ni_cMg_{1-c}O$ system, according the elastic magnetic neutron scattering [11] and SQUID magnetometry [11,12]. The region of infinite antiferromagnetic cluster [13] is indicated by open squares. *P* means paramagnetic region, AF — antiferromagnetic region, CSG — cluster spin-glass.

which shed light on magnetic interactions in $Ni_cMg_{1-c}O$ at the microscopic level.

2. Samples preparation and experimental techniques

The $Ni_cMg_{1-c}O$ samples used in the present work were green coloured polycrystalline powders or single-crystals [9,10]. Polycrystalline solid solutions were prepared using ceramic technology from the appropriate amounts of aqueous solutions of $Mg(NO_3)_2 \cdot 6H_2O$ and $Ni(NO_3)_2 \cdot 6H_2O$ salts, which were mixed and slowly evaporated. The ramaining dry „flakes" were heated up to 500–600°C to remove NO_2 completely. The obtained polycrystalline solid solutions were pressed and annealed during 100 h at 1200°C in air and then rapidly cooled down to room temperature. $Ni_cMg_{1-c}O$ single-crystals were grown by the method of chemical transport reactions (the „sandwich" technique) on the (100) face of MgO single-crystals. The chemical composition of samples was controlled by instrumental neutron-activated analysis [14]: the content of nickel was in agreement with the stoichiometric one within $\pm 0.01\%$. The obtained $Ni_cMg_{1-c}O$ solid solutions were studied by several experimental techniques: IR–VIS optical absorption [15–17], photoluminescence [18–22] and Raman spectroscopies [23,24], X-ray [25] and neutron [11] diffraction, X-ray absorption spectroscopy (XAS) [26–28]. The details of the experiments are available from the corresponding references.

3. Results and discussion

First, let us discuss the influence of magnetic interaction on the crystallographic structure of $Ni_cMg_{1-c}O$ solid solutions, whose continuous series can be prepared due to a small difference (about 0.02 Å) of the ionic radii of Ni^{2+} and Mg^{2+} ions [9,10]. It was believed for a long time that the lattice parameter of $Ni_cMg_{1-c}O$ system depends linearly on the composition and follows the Vegard's rule: $a(c) = ca_{NiO} + (1-c)a_{MgO}$ [9,12,29,30]. However, the results of the Ni K-edge XAS studies [26,27] suggested a deviation of the local environment a round Ni^{2+} ions from the Vegard's model. It was observed that while the nearest interatomic Ni–O and Ni–Mg distances change linearly, according to the Vegard's model, the nearest Ni–Ni distance remains nearly constant at all compositions [26,27]. This results stimulated more accurate X-ray diffraction (XRD) study [25], which confirmed the XAS findings. It was determined that the values of the lattice parameter $a(c)$ in the $Ni_cMg_{1-c}O$ series differ from the ones predicted by the Vegard's model, and the maximum deviation is about -0.002 Å for $c \sim 0.4$ (Fig. 2) [25]. Note that such $a(c)$ dependence can be well fitted by the model assuming constant nearest Ni–Ni distance [25]. Thus, both XRD and XAS experiments suggest a distortion of the local environment around nickel ion, which progressively increases upon dilution with magnesium ions. The origin of such distortion is attributed to the exchange interaction between neighbouring nickel ions, causing them to displace to off-center position. We correlate a symmetry lowering at nickel ions sites with the observed splitting of the zero-phonon line in the low-temperature optical absorption and photoluminescence spectra of $Ni_cMg_{1-c}O$ for $c \leq 0.2$ in the energy range 7800–8300 cm^{-1} of $^3A_{2g} \leftrightarrow {}^2T_{2g}$ band [21]. The existence of the two sharp zero-phonon lines (E and T) in $^3A_{2g} \leftrightarrow {}^3T_{2g}$ band at 8005 and 8182 cm^{-1} has been traditionally explained by the spin-orbit splitting [18,19,20,31]. However, according to the calculations [31], the four zero-phonon lines are expected with the relative intensities equal to 0.677, 1.000, 0.790 and 0.235, while only two lines with the relative intensities equal to 0.645, 1.000 are observed in the experiment [18–21]. Moreover, it is known that at the nickel concentrations $0.01 < c < 0.2$, additional zero-phonon lines appears at 7822, 7888, 7921 and 7937 cm^{-1} which are attributed to the exchange-coupled Ni^{2+}–Ni^{2+} pairs, which are formed due to the 90° superexchange Ni^{2+}–O^{2-}–Ni^{2+} interactions [19–21]. The maximum number of isolated pairs is observed at $c = 0.05$, and they aggregate into clusters at higher nickel concentrations [20,21].

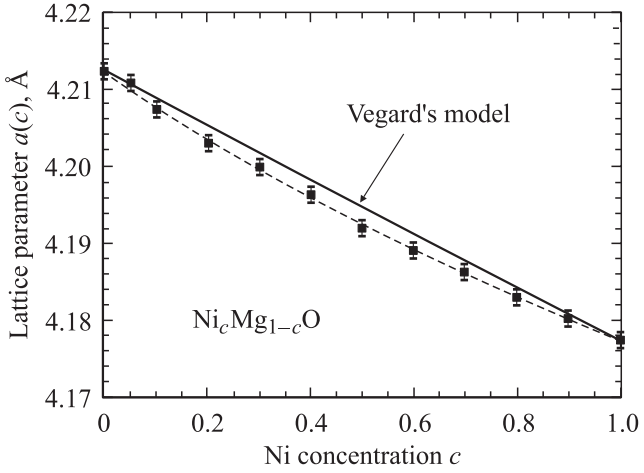

Figure 2. Variation of the lattice parameter $a(c)$ (shown by points) in $Ni_cMg_{1-c}O$ [25]. Solid line shown linear Vegard's model. Dashed line corresponds to the model $a(c) = c^2 a_{NiO} + 2c(1-c)(b_1 + b_2 c) + (1-c)^2(ca_{NiO} + (1-c)a_{MgO})$ with $b_1 = 4.206$ Å and $b_2 = -0.014$ Å, taking into account a displacement of nickel atoms upon dilution by magnesium [25].

The optical properties of the $Ni_cMg_{1-c}O$ solid solutions with small concentration of nickel ions was studied in details in the past [18–21,32–34]. Therefore, we will discuss further the case of high nickel content ($c > 0.05$). The optical absorption spectra of $Ni_cMg_{1-c}O$ solid solutions can be interpreted using the energy level diagram of a free nickel ion $Ni^{2+}(3d^8)$ in a cubic crystal field. The observed absorption bands (Fig. 3) are related to the parity-forbidden $d-d$ transitions, three of which, $^3A_{2g}(F) \rightarrow {}^3T_{2g}(F)$, $^3A_{2g}(F) \rightarrow {}^3T_{1g}(F)$ and $^3A_{2g}(F) \rightarrow {}^3T_{1g}(P)$, are spin-allowed ($\Delta S = 0$), whereas the others are forbidden. We will consider the two lowest bands, which correspond to the magnetic-dipole transition

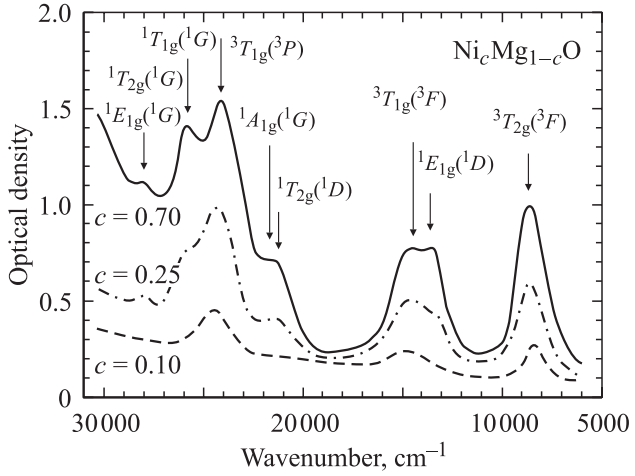

Figure 3. Room temperature optical absorption in $Ni_cMg_{1-c}O$ single-crystals [10].

$^3A_{2g}(F) \rightarrow {}^3T_{2g}(F)$ at $\sim 8800\,\mathrm{cm}^{-1}$ and the electric-dipole transition $^3A_{2g}(F) \rightarrow {}^1E_g(D)$ at $\sim 13\,800\,\mathrm{cm}^{-1}$. Note that both bands are sensitive to the magnetic ordering.

At low temperature, the magnetic-dipole band $^3A_{2g}(F) \rightarrow {}^3T_{2g}(F)$ consists of two sharp zero-phonon lines (peaks A and B in Fig. 4), phonon satellite peaks and broad sideband [16,19]. The peak A at $\sim 7800\,\mathrm{cm}^{-1}$ is assigned to the pure exciton transition whereas the peak B at $\sim 7840\,\mathrm{cm}^{-1}$ — to the exciton–one-magnon excitation [16,19]. Here the one-magnon excitation occurs at the Brillouin zone-center (BZC), and its energy is defined by the difference between peaks A and B. Upon temperature change or substitution of nickel ions with magnesium ones, the band experiences homogeneous and inhomogeneous broadening which influences the intensity and the position of both peaks and of the phonon sideband [35]. An introduction of less than 10% of magnesium ions ($c > 0.9$) results in a strong damping of the peak B intensity already at $T = 6\,\mathrm{K}$, that is very far below the Nèel temperature (Fig. 1). Within the accuracy of our experimental data, the one-magnon energy in $Ni_cMg_{1-c}O$ for $c > 0.95$ is nearly unchanged and equals to that of pure NiO $\omega_{1M} \approx 41\,\mathrm{cm}^{-1}$. There is also some evidence for a decrease of ω_{1M} by $\sim 8\,\mathrm{cm}^{-1}$ for $c = 0.95$ (Fig. 4). Note that similar variation of ω_{1M} with composition has been observed recently in the one-magnon Raman scattering [24]. For $c \leq 0.9$ the one-magnon contribution cannot be detected as a distinct peak at 6 K, however a shoulder at the place of peaks A and B is visible in $Ni_{0.90}Mg_{0.10}O$ (Fig. 4). According to the magnetic phase diagram (Fig. 1), the antiferromagnetic ordering in $Ni_cMg_{1-c}O$ exists [11,12] at $T = 6\,\mathrm{K}$ for $c \geq \sim 0.4$ and, moreover, an infinite antiferromagnetic domain structure is observable for $c > \sim 0.6$ [13]. In pure or lightly-doped NiO, an infinite antiferromagnetic domain structure is present till $\sim 450\,\mathrm{K}$ [13], and the antiferromagnetic ordering remains up to 523 K. However, these results reflect the macroscopic magnetic properties of NiO and $Ni_cMg_{1-c}O$, whereas optical spectroscopy provides with the microscopic

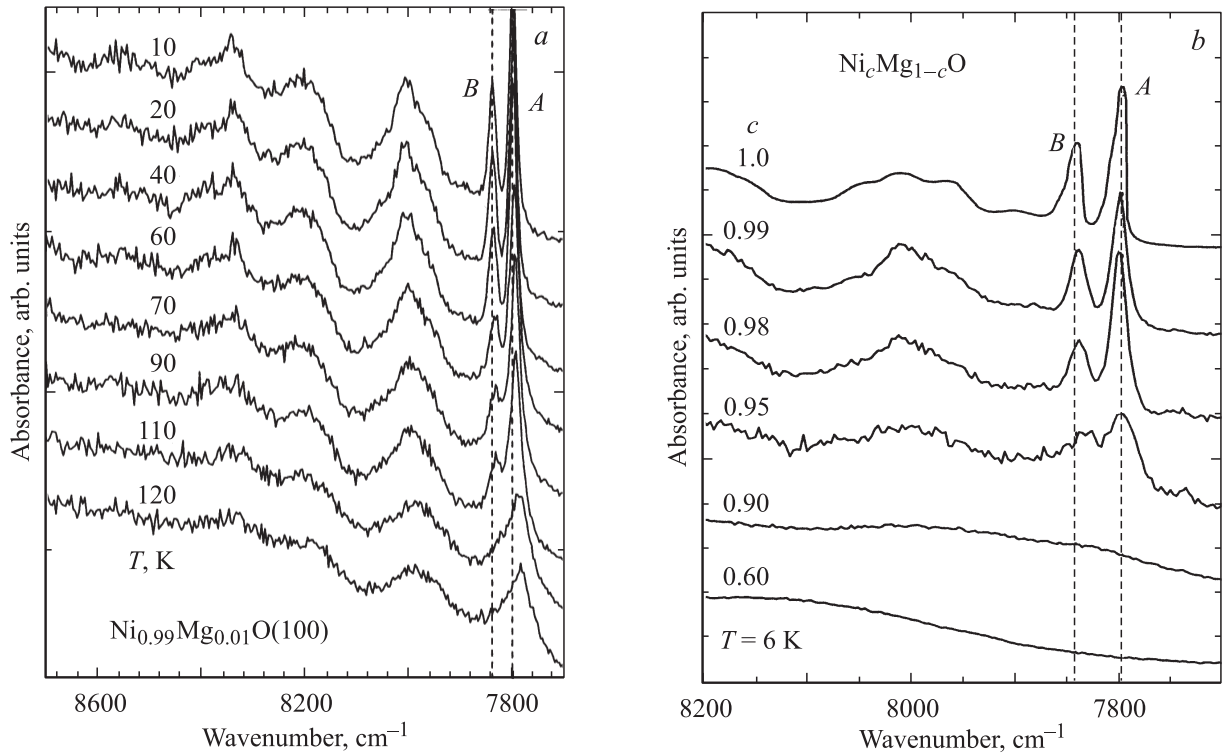

Figure 4. Temperature (a) and concentration (b) dependences of the low-energy part of the $^3A_{2g}(F) \rightarrow {}^3T_{2g}(F)$ absorption band in $Ni_cMg_{1-c}O$ single-crystals [16]. The peaks due to the pure excition transition and exciton–one-magnon excitation are indicated by the letters A and B, respectively.

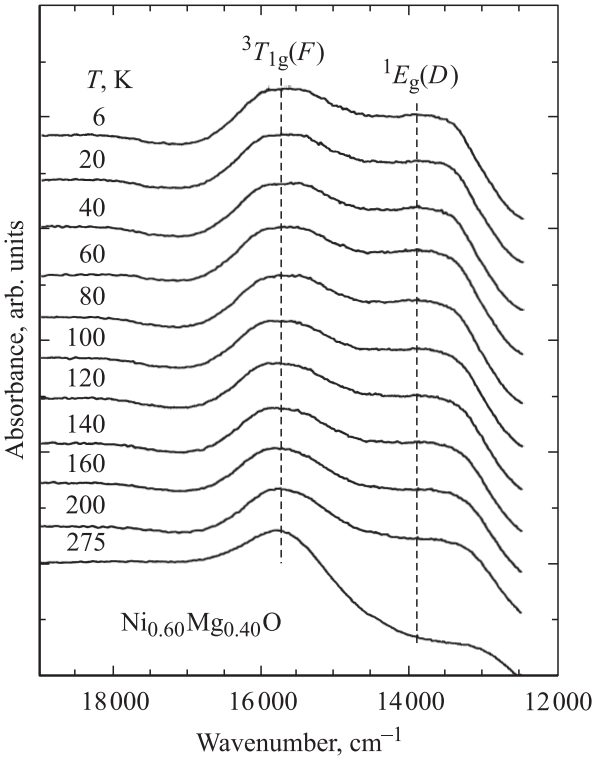

Figure 5. Temperature dependences of $^3A_{2g}(F) \rightarrow {}^3T_{1g}(F)$, $^1E_g(D)$ absorption bands in $Ni_{0.60}Mg_{0.40}O$ single-crystals [16].

point of view. Our results indicate that long-wavelength BZC magnons are very sensitive to a disturbance of long-range spin-spin correlations due to temperature increase or dilution by non-magnetic ions.

Temperature dependence of the electric-dipole transition $^3A_{2g}(F) \rightarrow {}^1E_g(D)$ in $Ni_{0.60}Mg_{0.40}O$ is shown in Fig. 5, and a variation of the band with composition — in Fig. 3. Note that the $^1E_g(D)$ band overlaps partially with the $^3T_{1g}(F)$ band located at $\sim 15\,700\,\text{cm}^{-1}$. The intensity of the $^1E_g(D)$ band for $c = 0.60$ experiences an abrupt decrease in the temperature interval 200–275 K, just below the Nèel temperature $T_N \sim 320$ K (Fig. 5). At room temperature, the abrupt change occurs between $c = 0.25$ and 0.7 (Fig. 3). Our previous study [36] of this band in $KNiF_3$ single-crystal suggests that the $^1E_g(D)$ band has complex structure, consisting of the exciton–photon background and the exciton–two-magnon contribution sitting on it. The pure exciton transition is parity- and spin-forbidden, so it is not visible in the experimental data, but is expected to be at $\sim 12\,500\,\text{cm}^{-1}$. The two magnons are excited at the Brillouin zone-boundary (BZB), so that they are short-wavelength magnons and, thus, are sensitive to the short-range magnetic ordering. As a result, the two-magnon contribution remains visible up to T_N (Fig. 5). Similar behaviour for two-magnon contribution was also found in Raman spectra of NiO [37] and $KNiF_3$ [38]. The two-magnon energy ω_{2M} can be roughly estimated to be $\sim 1400\,\text{cm}^{-1}$, that is much larger than in $KNiF_3$ ($\omega_{2M} = 813\,\text{cm}^{-1}$) due to the stronger superexchange interactions between Ni^{2+} ions.

Contrary to the optical absorption spectra (Fig. 3), where several bands due to intra Ni_{2+} ion transitions are observed (Fig. 3), the photoluminescence spectra [22] in the range 11 000–22 000 cm^{-1} at high nickel concentrations consist of only two broad bands (Fig. 6): the red band at 12 500 cm^{-1} and the green band at 18 500 cm^{-1}. The intensity of both bands decreases with increasing temperature but is still detectable at room temperature. Besides, we found that the intensities ratio for the two bands depends strongly on the sample composition and the excitation laser wavelength [22]. We attribute the two bands to the impurity- or defect-perturbed Ni^{2+} states, similar to that observed [39,40] in MnO and MnS. The band at 12 500 cm^{-1} is related to the transitions from some defect levels located in the gap between $^3T_{1g}(F)$ and $^1T_{2g}(D)$ Ni^{2+} levels. Similarly, the position of the red band is attributed to the defect levels

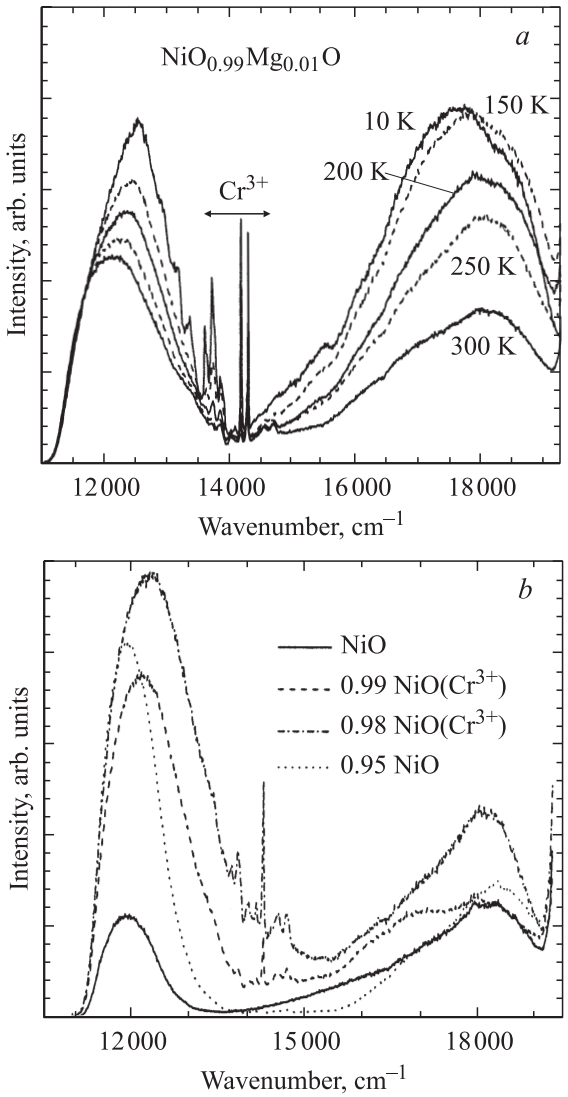

Figure 6. Temperature (a) and composition (at room temperature) (b) dependences of the photoluminescence in $Ni_cMg_{1-c}O$ solid solutions under the 514 nm excitation laser wavelength [22]. The luminescence due to Cr^{3+} ions comes from the MgO substrate.

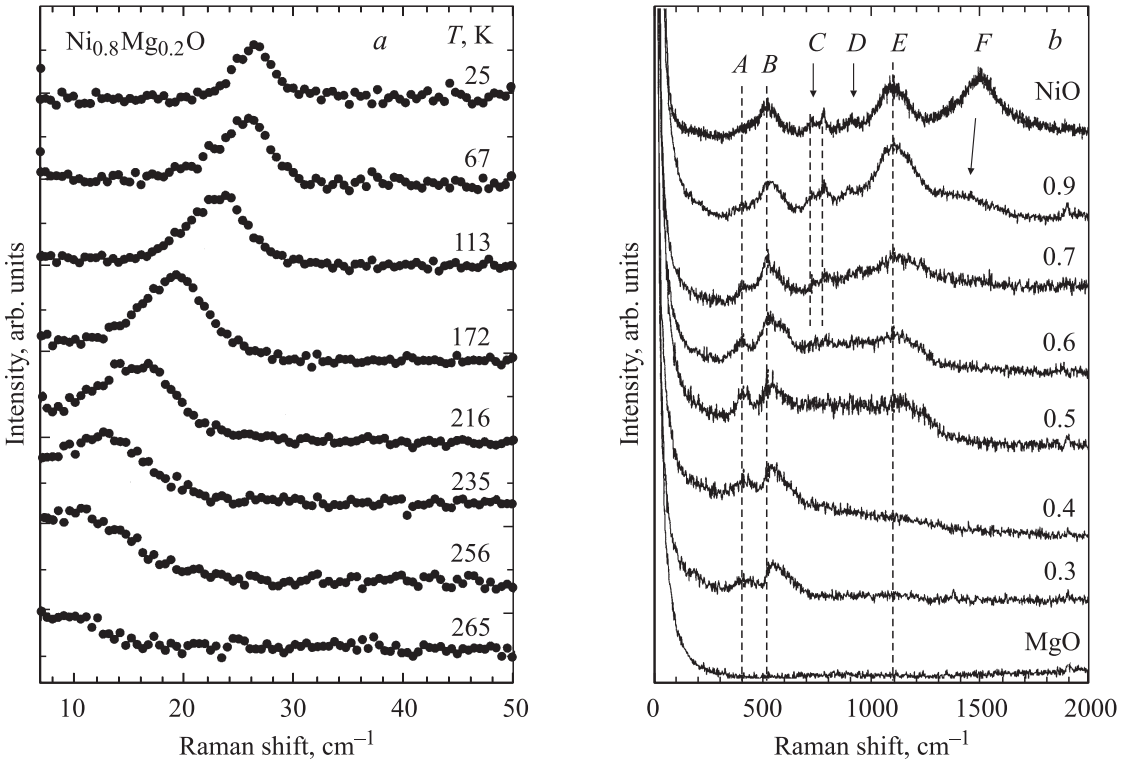

Figure 7. *a*) Temperature dependence of the one-magnon Raman scattering in $Ni_{0.80}Mg_{0.20}O$ solid solution [24]. *b*) Composition dependence of the room temperature Raman spectra of polycrystalline $Ni_cMg_{1-c}O$ solid solutions [23]. The origin of the peaks $A-F$ is explained in text. The spectral intensities are scaled so that one-phonon scattering in the different spectra turns out roughly comparable.

located in the gap between ${}^3T_{2g}(F)$ and ${}^1E_g(D)$ Ni^{2+} levels. The observed luminescence bands experience inhomogeneous and homogeneous broadening due to compositional disorder, exciton–phonon and exciton–magnon interactions. The intensity of the bands is also determined by an off-centre displacement of nickel ions due to substitution by magnesium.

The room temperature Raman spectrum of pure NiO consists of several bands (Fig. 7): a one-magnon ($1M$) band [41] at $34\,cm^{-1}$, five vibrational bands [6] — one-phonon ($1P$) TO (at $440\,cm^{-1}$, peak A) and LO (at $560\,cm^{-1}$, peak B) modes, two-phonon ($2P$) $2TO$ modes (at $740\,cm^{-1}$, peak C), $TO+LO$ (at $925\,cm^{-1}$, peak D) and $2LO$ (at $1100\,cm^{-1}$, peak E) modes, and a two-magnon ($2M$) band F at $\sim 1500\,cm^{-1}$. The frequency and shape of the phonon bands do not vary with temperature, whereas the magnon scattering intnsities are strongly temperature-dependent: they shift to lower frequencies and decrease in intensity with increasing temperature, desappearing completely close to the Nèel point [6,41].

The one-magnon Raman scattering measured for $c \geq 0.6$ is shown in Fig. 7, *a* for $Ni_{0.8}Mg_{0.2}O$ solid solution [24]. Here it can be detected up to about 270 K, and the one-magnon frequency extrapolated to $T = 0\,K$ is about $26 \pm 1\,cm^{-1}$. As it is expected, the one-magnon frequency decreases and the peak progressively broadens upon increasing temperature. The extrapolation of the temperature dependence of the one-magnon frequency to $\omega_{1M} = 0$ gives the critical temperature $T_C \approx 300\,K$, that is much smaller than the Nèel temperature [11] $T_N(c = 0.8) \approx 420\,K$. The analysis of one-magnon Raman scattering for other compositions allowed us to conclude that (*a*) the one-magnon frequency extrapolated to $T = 0\,K$ experiences an abrupt change between $c = 0.99$ and 0.9 and (*b*) the one-magnon energy for highly diluted nickel oxide vanishes significantly below the Nèel temperature. The abrupt change of the one-magnon frequency at $T = 0\,K$ with compsition is unexpected and requires further studies. Also the behaviour of the one-magnon frequency close to the Nèel temperature requires clarification.

Room temperature Raman spectra of polycrystalline $Ni_cMg_{1-c}O$ solid solutions are shown in Fig. 7, *b* [24]. The most exciting result is concerned with the strong decrease of the two-phonon band intensity relative to the one-phonon contribution for small nickel concentrations. As one can see, upon dilution with magnesium ions, the one-phonon bands A and B change slightly in shape: mainly, the band A becomes more pronounced. At the same time, the two-phonon bands C, D and E broaden up for $0.5 \leq c < 0.9$ and disappear completely for $c \leq 0.4$. Since the crystalline structure of $Ni_cMg_{1-c}O$ solid solutions follows that of NiO and MgO, no significant changes of the phonon density of states are expected [24]. Therefore, we suggest that for increasing magnesium concentration the first-order Raman scattering becomes more and more allowed due to lowering of local symmetry at Ni^{2+} sites caused by two effects —

composition disorder and off-centre displacement of nickel ions. The intensity of the two-magnon band F decreases with increasing magnesium concentration, and its position shifts to the lower frequencies as expected. In fact, the two-magnon band F becomes located under the phonon bands and could be partially responsible for the background contribution for $c < 0.7$.

4. Summary and conclusions

We have reviewed the recent experimental data together with their interpretation for $Ni_cMg_{1-c}O$ solid solutions with an emphasis on the exchange interactions between Ni^{2+} ions. We have shown that different experimental methods provide with complementary information and allow deeper understanding of $Ni_cMg_{1-c}O$ system. It was found that dilution of nickel oxide with magnesium ions affects strongly atomic structure and optical, magnetic and vibrational properties. Opposite to conventional point of view, the local symmetry at Ni^{2+} ions sites does lower upon dilution due to magnetic interactions beween neighbouring nickel ions. The magnetic interactions can be accessed through the study of optical and Raman spectroscopy, since both one-magnon and two-magnon excitations contribute strongly to optical and Raman spectra. We found that the one-magnon energy depending on composition show an unexpected trend which can be explained by a strong decrease of the spin-spin correlation length upon dilution. However further studies are required to fully understand this behaviour.

References

[1] W. Giriat, J.K. Furdyna. In: Semiconductors and Semimetals. Vol. 25. / Ed. J.K. Furdyna, J. Kossut. Academic Press, N.Y. (1988).
[2] J.B. Goodenough. Magnetism and the Chemical Bond. Interscience Publishers, N.Y. (1963).
[3] W.L. Roth. Phys. Rev. **110**, 1333 (1958).
[4] M.T. Hutchings, E.J. Samuelsen. Phys. Rev. B **6**, 3447 (1972).
[5] F.U. Hillebrecht, H. Ohldag, N.B. Weber, C. Bethke, U. Mick, M. Weiss, J. Bahrdt. Phys. Rev. Lett. **86**, 3419 (2001).
[6] R.E. Dietz, W.F. Brinkman, A.E. Meixner, H.J. Guggenheim. Phys. Rev. Lett. **27**, 814 (1971).
[7] M.J Massey, N.H. Chen, J.W. Allen, R. Merlin. Phys. Rev. B **42**, 8776 (1990).
[8] M. Fiebig, D. Fröhlich, Th. Lottermoser, V.V. Pavlov, R.V. Pisarev, H.-J. Weber. Phys. Rev. Lett. **87**, 137 202 (2001).
[9] N.A. Mironova, G.V. Bandurkina. Izv, Akad. Nauk LatvSSR. Ser. Fiz. Tech. Nauk *4*, 14 (1975).
[10] N.A. Mironova, U.A. Ulmanis. Radiation Defects and Metal Ions of Iron Group in Oxides. Zinatne, Riga (1988).
[11] A.Z. Menshikov, Yu.A. Dorofeev, A.G. Klimenko, N.A. Mironova. Phys. Stat. Sol. (b) **164**, 275 (1991).
[12] Z. Feng, M.S. Seehra. Phys. Rev. B **45**, 2184 (1992).
[13] N.A. Mironova, A.I. Belyaeva, O.V. Miloslavskaya, G.V. Bandurkina. Ukr. Fiz. Zh. **34**, 848 (1981).
[14] D.V. Riekstina, I.E. Cirkunova, G.J. Eglite. Izv. Akad. Nauk LatvSSR. Ser. Fiz. Tech. Nauk *1*, 3 (1975).
[15] N.A. Mironova, G.A. Grinvald, V.N. Skvortsova, U.A. Ulmanis. Sov. Phys. Solid State **23**, 874 (1981).
[16] N. Mironova-Ulmane, V. Skvortsova, A. Kuzmin, I. Sildos. Phys. Solid State **44**, 1403 (2002).
[17] N. Mironova-Ulmane, A. Kuzmin, M. Cestelli Guidi, M. Piccinini, A. Marcelli. Phys. Stat. Sol. (c). In press (2005).
[18] G.A. Grinvald, N.A. Mironova. Izv. Akad. Nauk LatvSSR. Ser. Fiz. Tech. Nauk *4*, 79 (1978).
[19] G.A. Grinvald, N.A. Mironova. Izv. Akad. Nauk LatvSSR. Ser. Fiz. Tech. Nauk *1*, 28 (1983).
[20] G.A. Grinvald, N.A. Mironova. Phys. Stat. Sol. (b) **99**, K101 (1980).
[21] N. Mironova, V. Skvortsova, A. Kuzmin, J. Porans. J. Lumin. **72–74**, 231 (1997).
[22] A. Kuzmin, N. Mironova-Ulmane, S. Ronchin. Proc. SPIE **5122**, 61 (2003).
[23] E. Cazzanelli, A. Kuzmin, G. Mariotto, N. Mironova-Ulmane. J. Phys.: Cond. Matter **15**, 2045 (2003).
[24] E. Cazzanelli, A. Kuzmin, G. Mariotto, N. Mironova-Ulmane. Phys. Stat. Sol. (c). In press (2005).
[25] A. Kuzmin, N. Mironova. J. Phys.: Cond. Matter **10**, 7937 (1998).
[26] A. Kuzmin, N. Mironova, J. Purans, A. Rodionov. J. Phys.: Cond. Matter **7**, 9357 (1995).
[27] A. Kuzmin, N. Mironova, J. Purans. J. Phys.: Cond. Matter **9**, 5277 (1997).
[28] A. Kuzmin, J. Purans, R. Kalendarev. Phys. Stat. Sol. (c). In press. (2005).
[29] W.C. Hahn, J.A. Muan. J. Phys. Chem. Sol. **19**, 338 (1961).
[30] T. Yoshida, T. Tanaka, H. Yoshida, T. Funabiki, S. Yoshida. J. Phys. Chem. **100**, 2302 (1996).
[31] K.Y. Wong, D. Sengupta, E.R. Krausz. Chem. Phys. Lett. **21**, 137 (1973).
[32] R. Pappalardo, D.L. Wood, R.C. Linares, jr. J. Chem. Phys. **35**, 1460 (1961).
[33] J.E. Ralph, M.G. Townsend. J. Chem. Phys. **48** 149 (1968).
[34] J.E. Ralph, M.G. Townsend. J. Phys. C: Solid State Phys. **3**, 8 (1970).
[35] K.K. Rebane. In: Zero-Photon Lines and Spectral Hole Burning in Spectroscopy and Photochemistry / Ed. O. Sild, K. Haller. Springer, Berlin (1988). P. 1–18.
[36] N. Mironova-Ulmane, V. Skvortsova, A. Kuzmin, I. Sildos. Ferroelectrics **258**, 177 (2001).
[37] R.E. Dietz, G.I. Parisot, A.E. Meixner. Phys. Rev. B **4**, 2302 (1971).
[38] S.R. Chinn, H.J. Zeiger, J.R. O'Connor. Phys. Rev. B **3**, 1709 (1971).
[39] S. Mochizuki, B. Piriou, J. Dexpert-Ghys. J. Phys.: Cond. Matter **2**, 5225 (1990).
[40] S. Mochizuki. J. Phys.: Cond. Matter **2**, 7225 (1990).
[41] D.J. Lockwood, M.G. Cottam, J.H. Baskey. J. Magn. Magn. Mater. **104–107**, 1053 (1992).